TABLE 3 Performance Comparison With Previous Works

	This work	[1]	[2]	[3]	[4]	[5]	[6]
f_0 (GHz)	2.6	2.4	1	1	1.5	1.5	2.6
Ter. Imp. (Ω)	50–25	50	50	50	50	50	50
FBW (%)	20*	9.2†	13*	17*	35*	54*	20.76
Phase diff.	180° ± 5°	180 °± 1°	180 °± 5°	180° ± 5°	180° ± 10°	180° ± 3.4°	180° ± 5°
Isolation (dB)	19 (FBW=24.6%)	NA	NA	NA	NA	NA	18 (FBW=28%)
Circuit size (mm^2)	35 × 55	NA	NA	NA	15.9 × 15.9	29 × 30.5	60 × 60

*−19 dB S11 FBW.
†−12.2 dB S_{11} FBW, Ter. Imp.: termination impedance.

center frequency (f_o). Moreover, the wideband characteristic is found in the under-matched region compared to the perfect and over-matched regions.

The design steps of the proposed balun are as follows.

a. First, specify Z_{0o}, Z_1, f_0, Z_L, Z_S, $S_{23}|_{f0}$, and $S_{11o}|_{f0}$ for all matched regions.
b. For the perfect matched region, calculate Z_t using Eq. (4). Then calculate Z_{0e} and R using Eqs. (7) and (11), respectively.
c. For the over-matched region, calculate Z_t using Eq. (5). Then calculate Z_{0e} and R using Eqs. (7) and (12), respectively.
d. For the under-matched region, calculate Z_t using Eq. (6). Then calculate Z_{0e} and R using Eqs. (7) and (13), respectively.
e. Finally, obtain the physical dimensions of the coupled lines according to PCB substrate from RF circuit simulator and optimize using electromagnetic (EM) simulator.

3. SIMULATION AND MEASUREMENT RESULTS

To demonstrate and validate the analysis, the branch-line balun was designed at an f_o of 2.6 GHz. The designed values of $S_{11o}|_{f0}$ and $S_{23}|_{f0}$ are −20 dB with 50–25 Ω termination impedances. The under-matched region was chosen for wideband characteristics. The circuit was fabricated on RT/Duroid 5880 substrate with $\varepsilon_r = 2.2$ and $h = 31$ mils. EM simulation was performed using ANSYS HFSS v15.

Figure 5 shows the EM simulation layout and a photograph of the fabricated balun. The circuit size is 35 ×× 55 mm^2 ignoring the impedance transformer to match with 50 Ω for the measurement. The physical dimensions and component value are shown in Table 2.

Figure 6 shows the simulation and measurement results of the fabricated balun. From the measurement, the return loss is obtained as 22.3 dB at f_0. The bandwidth of 20 dB return loss is 0.51 GHz (2.39–2.9 GHz). The measured results are in good agreement with the simulations. The measured power divisions are −3.29 dB and −3.3 dB at f_0, respectively. The amplitude division of -3 ± 0.6 dB is obtained within the bandwidth of 0.51 GHz. The isolation between the output ports is obtained as 20.05 dB at f_0. Isolation higher than 19 dB is obtained over a bandwidth of 0.64 GHz (2.3–2.94 GHz). The measured phase imbalance between two output ports is 180° ± 5° over the bandwidth of 0.64 GHz. The performance comparisons are summarized in Table 3.

The proposed balun provided wideband and high isolation characteristics with unequal termination impedance. The circuit size of the proposed work is much improved when compared with Ref. 6.

4. CONCLUSION

In this article, a branch-line balun was proposed. Shunt coupled lines with a resistor between the output ports were used to obtain wideband and high isolation characteristics. The measurement results are in good agreement with simulation results. The proposed structure is simple to design and fabricate and is applicable for wideband RF systems.

ACKNOWLEDGMENT

This research was supported by "Research Base Construction Fund Support Program" Funded by Chonbuk National University in 2015.

REFERENCES

1. Y. Leong, K. Ang, and C. Lee, A derivation of a class of 3-port baluns from symmetrical 4-port networks, IEEE MTT-S Int Microwave Symp Dig, Seattle, WA (2002), 1165–1168.
2. M. Park and B. Lee, Stubbed branch-line balun, IEEE Microwave Wireless Compon Lett 17 (2007), 169–171.
3. M. Zhou, J. Shao, B. Arigong, H. Ren, J. Ding, and H. Zhang, Design of microwave baluns with flexible structures, IEEE Microwave Wireless Compon Lett 24 (2014), 695–697.
4. J. Li, S. Qu, and Q. Xue, Miniaturised branch-line balun with bandwidth enhancement, Electron Lett 43 (2007), 931–932.
5. H. Xu, G. Wang, X. Chen, and T. Li, Broadband balun using fully artificial fractal-shaped composite right/left handed transmission line, IEEE Microwave Wireless Compon Lett 22 (2012), 16–18.
6. P. Kim, G. Chaudhary, and Y. Jeong, Analysis and design of a branch line balun with high-isolation wideband characteristics, Microwave Opt Technol Lett 57 (2015), 1228–1234.
7. H. Ahn, Asymmetric passive components in microwave integrated circuits, Wiley, Hoboken, NJ, 2006, pp. 154–167.

UNCONDITIONALLY STABLE FDTD SCATTERED FIELD FORMULATION FOR DISPERSIVE MEDIA

Hasan Khaled Rouf[1] and Daniel Erni[2]
[1] Department of Applied Physics, Electronics and Communication Engineering, University of Chittagong, Chittagong 4331, Bangladesh; Corresponding author: hasan.rouf@cu.ac.bd
[2] General and Theoretical Electrical Engineering (ATE), Faculty of Engineering, University of Duisburg-Essen, and CENIDE - Center for Nanointegration Duisburg-Essen, Duisburg 47048, Germany

Received 13 December 2015

ABSTRACT: *A new unconditionally stable scattered field (SF) formulation for the finite difference time domain (FDTD) technique applied to dispersive media is presented. The scheme is based on alternating direction implicit (ADI) principle but, unlike ADI, it does not require computation and storage of field values at the intermediate time steps which reduces computational costs and memory. Dispersive media characterized by Debye and Lorentz models are incorporated in the proposed SF FDTD scheme by auxiliary differential equation (ADE) method. For each of the dispersive media unconditional stability and accuracy of the scheme are validated by numerical tests. The scheme can perform faster*

than the explicit FDTD scheme at Courant number as low as three.
 Microwave Opt Technol Lett 58:1778–1782, 2016; View this article online at wileyonlinelibrary.com. DOI 10.1002/mop.29963

Key words: *finite difference time domain; scattered field techniques; frequency dispersive media; unconditionally stable methods; computational electromagnetics*

1. INTRODUCTION

To solve electromagnetic scattering problems the finite difference time domain (FDTD) method is one of the most widely used numerical techniques. In such problems a spatially finite scatterer is illuminated by plane wave which is typically introduced by total field/scattered field (TFSF) [1] or scattered field (SF) approaches [2]. In the SF approach, the incident field components are specified analytically throughout the problem space while the scattered fields are found computationally. Incident and scattered fields must satisfy the Maxwell's equations independently. If the total field FDTD equations are desired, they can be obtained from the SF equations by setting the incident field to zero and applying the initial conditions to the scattered field. Conversely, the total field formulation does not separate the field into incident and scattered components, but treats only the total field when interaction with a scatterer is studied. In this approach propagates the incident wave propagates through the grid and therefore progressively accumulates errors due to numerical dispersion and anisotropy. SF approach does not suffer from this limitation as analytical functions are used to generate the incident wave at each field location.

Unlike the conventional (explicit) FDTD unconditionally stable implicit FDTD methods are not constrained by the Courant–Friedrich–Levy (CFL) stability criterion. In unconditionally stable schemes, the time-step size can be chosen independently from the spatial step size which renders significant computational advantage specially in applications where a very fine FDTD grid is needed for accurate modeling. A major breakthrough in unconditionally stable scheme was the alternating direction implicit (ADI-)FDTD method proposed by [3,4]. The ADI scheme splits each full FDTD step into two substeps, each involving solution of a tridiagonal matrix. To overcome the relatively large computational costs of the ADI method due to its substep computations, a leapfrog ADI-FDTD method was developed in [5] that does not require the mid-time computation. Unlike ADI this method solves for both electric and magnetic fields implicitly and in one direction only. In ADI-FDTD method the second step alternates the direction of update. Being a one-step method it requires less amount of memory and CPU time as computation and storage of field values at the intermediate step are not required. Reference [6] analytically proved its stability and presented the comparisons among various unconditionally stable implicit FDTD methods. It showed that the one-step leapfrog ADI-FDTD method was the most efficient among the recently developed unconditionally stable schemes. It found that both the conventional ADI-FDTD and the one-step leapfrog ADI-FDTD have the same numerical dispersion characteristics but the latter scheme requires the least amount of floating-point operations and memory.

Few works have been performed on scattered field FDTD formulation for the dispersive media. For example, [7] presented a SF formulation for Debye media based on the auxiliary differential equation (ADE) method while [8] used recursive convolution method to apply SF FDTD to Debye, Drude, and Lorentz materials. Reference [9] presented a SF formulation for Drude and Lorentz media. An SF FDTD technique for modeling scattering from dispersive objects residing in stratified dispersive media was proposed in [10]. However, despite many advantages of scattered field technique over total field technique, to our best knowledge, no scattered field unconditionally stable scheme has been developed so far for Debye and Lorentz media. Reference [11] presented an unconditioally stable SF FDTD algorithm for Drude dispersive medium.

In this article, a new scattered field unconditionally stable scheme is presented for Debye and Lorentz media. Although the scheme is based on ADI principle, it does not require the splitting in two substeps. It follows the approach of [5] which presented the total field formulation for a frequency independent medium. The scheme leads to one-step tridiagonal implicit equations but unlike ADI no mid-time field computation and storage is required which saves computational time and memory. We have adopted the ADE method to incorporate Debye-, and Lorentz-type dispersive media. The ADE technique translates the frequency-dependent constitutive relation in the time domain, by inverse Fourier transform, leading to an ordinary differential equation. A uniform implementation of different kinds of media has been adopted. To truncate the computational domain, we used convolutional perfectly matched layer (CPML) [12]. The scheme has been validated by numerical experiments and compared against exact analytical solutions. The scheme is unconditionally stable beyond CFL limit. By calculating the average relative errors at larger time-step sizes beyond the CFL limit we found that the scheme can maintain very good accuracy even when the Courant number is quite high. The proposed scheme becomes computationally more efficient than the explicit FDTD method when the Courant number is only at least three.

2. FORMULATION

In the practical applications of FDTD modeling Debye and Lorentz functions are widely used as they allow the simulation of frequency dependent electric permittivity variations of a range of materials including water, human tissues, gold, soils, etc. The permittivity of these two types of linear, isotropic dispersive media is as follows [1]:

$$\text{Debye model: } \varepsilon_r = \varepsilon_\infty + \sum_{p=1}^{P} \frac{\varepsilon_{s,p} - \varepsilon_{\infty,p}}{1 + j\omega T_{d,p}} \tag{1a}$$

where, $\varepsilon_{s,p}$ is the static or zero frequency relative permittivity, $\varepsilon_{\infty,p}$ is the relative permittivity at infinite frequency, $T_{d,p}$ is the pole relaxation time for pth pole and P is the number of poles in susceptibility response.

$$\text{Lorentz model : } \varepsilon_r(\omega) = \varepsilon_\infty + \sum_{p=1}^{P} \frac{\Delta\varepsilon_{l,p}\omega_{l,p}^2}{\omega_{l,p}^2 + 2j\omega\gamma_{l,p}\omega^2} \tag{1b}$$

where, $\Delta\varepsilon_{l,p}$ is the change in relative permittivity due to the Lorentz pole pair, $\omega_{l,p}$ is the Lorentz pole pair frequency, and $Y_{l,p}$ is the damping coefficient.

Now, the total electric and magnetic fields can be expressed as the sum of incident and scattered fields. That is: $\boldsymbol{E}_{\text{tot}} = \boldsymbol{E}_{\text{inc}} + \boldsymbol{E}_{\text{scat}}$ and $\boldsymbol{H}_{\text{tot}} = \boldsymbol{H}_{\text{inc}} + \boldsymbol{H}_{\text{scat}}$ where $\boldsymbol{E}_{\text{inc}}$ and $\boldsymbol{H}_{\text{inc}}$ are the values of the incident wave fields and $\boldsymbol{E}_{\text{scat}}$ and $\boldsymbol{H}_{\text{scat}}$ are the values of the scattered wave fields. In the SF technique incident wave fields are assumed to be known at all space points of FDTD grid and at all-time steps, whereas scattered wave fields are initially

unknown and arise from the interaction of the incident wave with any materials in the grid. In the SF technique, the FDTD method is used to time step only the scattered electric and magnetic fields. In the proposed algorithm, the incident field is specified to be propagating in free space for simplicity. Therefore, for the incident field in free-space Faraday's law, $\nabla\times\boldsymbol{E}=-\mu\frac{\partial \boldsymbol{H}}{\partial t}$, is given by $\nabla\times\boldsymbol{E}_{\text{inc}}=-\mu_0\frac{\partial \boldsymbol{H}_{\text{inc}}}{\partial t}$ For a dispersive medium, this equation is expressed as the total field: $\nabla\times\boldsymbol{E}_{\text{tot}}=-\mu\frac{\partial \boldsymbol{H}_{\text{tot}}}{\partial t}$ Taking $\mu=\mu_0$ for nonmagnetized medium and subtracting the former equation from the latter we obtain the scattered field expression:

$$\nabla\times\boldsymbol{E}_{\text{scat}}=-\mu\frac{\partial \boldsymbol{H}_{\text{scat}}}{\partial t} \tag{2}$$

We will use Ampère's law, $\nabla\times\boldsymbol{H}=j\omega\varepsilon_0\varepsilon_r(\omega)\boldsymbol{E}$, to relate electric field and polarization current density for the dispersive media. Thus, by substituting material permittivity from (1) in Ampère's law and then converting it to time domain we get

$$\nabla\times\boldsymbol{H}=\varepsilon_0\varepsilon_\infty\frac{\partial H}{\partial t}+J \tag{3}$$

where the expression for polarization current density $\boldsymbol{J}$ depends on the concerned dispersive medium and comes from manipulating (1) as follows:

For a single pole Debye medium

$$\boldsymbol{J}+T_d\frac{\partial \boldsymbol{J}}{\partial t}=\varepsilon_0(\varepsilon_s-\varepsilon_\infty)\frac{\partial E}{\partial t} \tag{4a}$$

while for a single pole Lorentz medium

$$\omega_l{}^2J+2\gamma_l\frac{\partial J}{\partial t}+\frac{\partial^2 J}{\partial t^2}=\varepsilon_0\Delta\varepsilon_l\omega_l{}^2\frac{\partial E}{\partial t} \tag{4b}$$

For an incident field in free space (3) can be written as $\nabla\times\boldsymbol{H}_{\text{inc}}=\varepsilon_0\frac{\partial \boldsymbol{E}_{\text{inc}}}{\partial t}$ whereas for a dispersive medium it becomes $\nabla\times\boldsymbol{H}_{\text{tot}}=\varepsilon_0\varepsilon_\infty\frac{\partial \boldsymbol{E}_{\text{tot}}}{\partial t}+\boldsymbol{J}_{\text{tot}}$. Subtraction of the former expression from the latter gives the scattered field expression for the propagating wave:

$$\nabla\times H_{\text{scat}}=\varepsilon_0\varepsilon_\infty\frac{\partial E_{\text{scat}}}{\partial t}+\varepsilon_0(\varepsilon_\infty-1)\frac{\partial E_{\text{inc}}}{\partial t}+J_{\text{tot}} \tag{5}$$

In vector differential Eqs. (2) and (5) the incident fields are defined analytically. Updating equations for the scattered field components $\boldsymbol{E}_{\text{scat}}$ and $\boldsymbol{H}_{\text{scat}}$ are obtained using the proposed unconditionally stable scheme. Like the ADI principle, for the substep from n to $n+1/2$ if we consider x-component of the electric field then (5) gives

$$E^{n+1/2}_{x,\text{scat}}=E^{n}_{x,\text{scat}}+aD_yH^{n+1/2}_{z,\text{scat}}-aD_zH^{n}_{y,\text{scat}}-c(E^{n+1/2}_{x,\text{inc}}-E^{n}_{x,\text{inc}})-aJ^{n+m_1}_{x,\text{tot}} \tag{6}$$

where $a=\Delta t/2\varepsilon_0\varepsilon_\infty$, $\mathbf{c}=(\varepsilon_\infty-\mathbf{1})/\varepsilon_\infty$, $D_w=\partial/\partial w$ $(w=x,y,z)$ and m_1 is the time index within the range of $[0,1/2]$ Again from (2) considering the z component of the magnetic field for the substep from n to $n+1/2$

$$H^{n+1/2}_{z,\text{scat}}=H^{n}_{z,\text{scat}}+bD_yE^{n+1/2}_{x,\text{scat}}-bD_xE^{n}_{y,\text{scat}} \tag{7}$$

where $b=\Delta t/2\mu$ Substituting (7) in (6) we get

$$\begin{aligned}(1-abD_{2y})E^{n+1/2}_{x,\text{scat}}=E^{n}_{x,\text{scat}}+a(D_yH^{n}_{z,\text{scat}}-D_zH^{n}_{y,\text{scat}})\\-abD_xD_yE^{n}_{y,\text{scat}}-c(E^{n+1/2}_{x,\text{inc}}-E^{n}_{x,\text{inc}})-aJ^{n+m_1}_{x,\text{tot}}\end{aligned} \tag{8}$$

Next $E_{x,\text{scat}}$ from (5) is discretized from substep $n+1/2$ to $n+1$

$$E^{n+1}_{x,\text{scat}}=E^{n+1/2}_{x,\text{scat}}+a(D_yH^{n+1/2}_{z,\text{scat}}-D_zH^{n+1}_{y,\text{scat}})-c(E^{n+1}_{x,\text{inc}}-E^{n+1/2}_{x,\text{inc}})-aJ^{n+m_2}_{x,\text{tot}} \tag{9}$$

where m_2 is the time index within the range of $[0,1/2]$ Again discretizing $H_{z,\text{scat}}$ in (2) from substep $n+1/2$ to $n+1$

$$H^{n+1}_{z,\text{scat}}=H^{n+1/2}_{z,\text{scat}}+b(D_yE^{n+1/2}_{x,\text{scat}}-D_xE^{n+1}_{y,\text{scat}}) \tag{10}$$

By substituting (10) in (9) and considering the previous time step, we get

$$\begin{aligned}E^{n}_{x,\text{scat}}=E^{n-1/2}_{x,\text{scat}}+a(D_yH^{n}_{z,\text{scat}}-D_zH^{n}_{y,\text{scat}})-ab(D_{2y}E^{n-1/2}_{x,\text{scat}}+D_yD_xE^{n}_{y,\text{scat}})\\-c(E^{n}_{x,\text{inc}}-E^{n-1/2}_{x,\text{inc}})-aJ^{n+m_2-1}_{x,\text{tot}}\end{aligned} \tag{11}$$

Finally, we substitute (11) into (8) and to avoid asymmetry error set both m_1 and m_2 to $1/2$ [13] which gives the expression of $E^{n+1/2}_{x,\text{scat}}$ in terms of $J_{x,\text{tot}}$ at current time step.

$$\begin{aligned}(1-abD_{2y})=E^{n+1/2}_{x,\text{scat}}=(1-abD_{2y})E^{n-1/2}_{x,\text{scat}}+2a(D_yH^{n}_{z,\text{scat}}-D_zH^{n}_{y,\text{scat}})\\-c(E^{n+1/2}_{x,\text{inc}}-E^{n-1/2}_{x,\text{inc}})-a(J^{n+1/2}_{x,\text{tot}}+J^{n-1/2}_{x,\text{tot}})\end{aligned} \tag{12}$$

Depending on whether the medium is of Debye- or Lorentz-type we get the expression for $J^{n+1/2}_{x,\text{tot}}$ from (4) and on substitution in (12) the final update equation for scattered electric field is obtained as follows.

For Debye medium

$$J^{n+1/2}_{x,\text{tot}}=\alpha J^{n-1/2}_{x,\text{tot}}+\beta(E^{n+1/2}_{x,\text{scat}}+E^{n+1/2}_{x,\text{inc}}-E^{n-1/2}_{x,\text{scat}}-E^{n+1/2}_{x,\text{inc}}) \tag{13}$$

where $\alpha=\frac{2T_d-\Delta t}{2T_d+\Delta t}$ and $\beta=\frac{2\varepsilon_0(\varepsilon_s-\varepsilon_\infty)}{2T_d+\Delta t}$

$$\begin{aligned}(1+\alpha\beta-abD_{2y})=E^{n+1/2}_{x,\text{scat}}=(1+\alpha\beta-abD_{2y})E^{n-1/2}_{x,\text{scat}}+2a(D_yH^{n}_{z,\text{scat}}-D_zH^{n}_{y,\text{scat}})\\-(c+\alpha\beta)(E^{n+1/2}_{x,\text{inc}}-E^{n-1/2}_{x,\text{inc}})-a(1+\alpha)J^{n-1/2}_{x,\text{tot}}\end{aligned} \tag{14}$$

For Lorentz medium

$$J^{n+1/2}_{x,\text{tot}}=\Gamma J^{n-1/2}_{x,\text{tot}}-\xi(J^{n-3/2}_{x,\text{tot}}+\boldsymbol{\zeta}(E^{n+1/2}_{x,\text{scat}}+E^{n+1/2}_{x,\text{inc}}-E^{n-1/2}_{x,\text{scat}}-E^{n-1/2}_{x,\text{inc}}) \tag{15}$$

where $\Gamma=\frac{4-\omega_l^2\Delta t^2+4\gamma_l\Delta t}{2+\omega_l^2\Delta t^2+4\gamma_l\Delta t}$, $\xi=\frac{2}{2+\omega_l^2\Delta t^2+4\gamma_l\Delta t}$, and $\zeta=\frac{2\varepsilon_0\Delta\varepsilon_l\omega_l^2\Delta t}{2+\omega_l^2\Delta t^2+4\gamma_l\Delta t}$

$$\begin{aligned}(1+a\zeta-abD_{2y})E^{n+1/2}_{x,\text{scat}}=(1+\alpha\zeta-abD_{2y})E^{n-1/2}_{x,\text{scat}}+2a(D_yH^{n}_{z,\text{scat}}-D_zH^{n}_{y,\text{scat}})\\-(c+\alpha\zeta)(E^{n+1/2}_{x,\text{inc}}-E^{n-1/2}_{x,\text{inc}})-a(1+\Gamma)J^{n-1/2}_{x,\text{tot}}+a\xi J^{n-3/2}_{x,\text{tot}}\end{aligned} \tag{16}$$

(14) and (16) are the final equations for calculating scattered electric fields depending on the concerned dispersive medium. They require the solution of a tridiagonal matrix only once at a

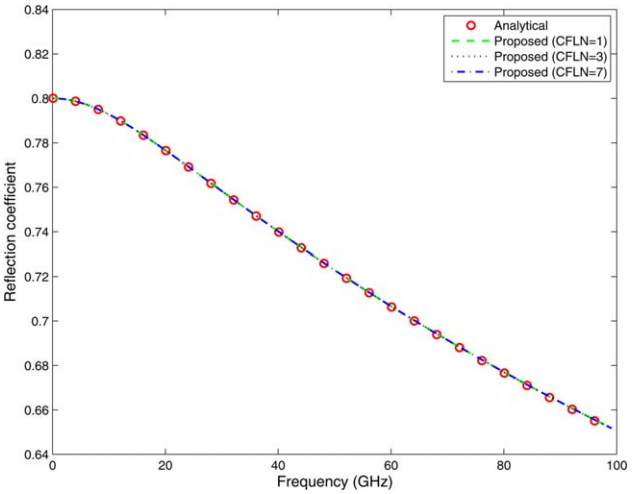

Figure 1 Reflection coefficient of an air–water interface computed by the proposed method at different CFLN The analytical solution is shown as reference. [Color figure can be viewed in the online issue, which is available at wileyonlinelibrary.com]

single time step. Calculation and storage of fields at the intermediate time step are not required. Depending on whether the concerned medium is of Debye- or Lorentz-type polarization current densities are calculated by using (13) and (15). The derivations for the magnetic fields are described now.

In the substep from n to $n+1/2$, from an equation similar to (6) but involving y-component of electric field $E^{n}_{y,\mathrm{scat}}$ is obtained and substituted in (7) to obtain $H^{n+1/2}_{z,\mathrm{scat}}$ Again in the substep from $n+1/2$ to $n+1$ $E^{n+1}_{y,\mathrm{scat}}$ is obtained similar to (9) and substituted in (10) to obtain $H^{n+1}_{z,\mathrm{scat}}$ in terms of $H^{n+1/2}_{z,\mathrm{scat}}$ Both of these equations involve $H^{n+1/2}_{z,\mathrm{scat}}$ and by combining them we get the final equation for the magnetic fields as follows:

$$(1-abD_{2x})H^{n+1}_{z,\mathrm{scat}}=(1-abD_{2x})H^{n+1}_{z,\mathrm{scat}}+2b(D_yE^{n+1/2}_{z,\mathrm{scat}}-D_xE^{n+1/2}_{y,\mathrm{scat}}) \tag{17}$$

Calculation of magnetic fields also requires the solution of a tridiagonal matrix at a single time step. For convenience, sequence of the complete procedure is summed up here:

- Solve (14) or (16) (depending on the concerned medium) and get the scattered electric fields.
- Solve (17) and get the scattered magnetic fields.
- Find the polarization density current from (13) or (15) (depending on the concerned medium).

3. NUMERICAL VALIDATION

The schemes presented in Section 2 are validated by numerical tests in this section. For the validation, we chose tests which have exact theoretical solutions. In particular, we calculated the reflection coefficient for a planar air-dispersive material interface and the transmittance of thin dispersive material slabs and compared both with the analytical solutions.

A typical first-order Debye material is water with the Debye parameters: $\varepsilon_s=81.0$, $\varepsilon_\infty=1.8$, $T_d=9.4\times10^{-12}$s. In the first test, we calculated the reflection coefficient when a plane wave is normally incident from vacuum onto water. In the numerical calculations the grid size is $\Delta s=14.97\mu$m and maximum time-step size allowed by the CFL limit is $\Delta t_{\mathrm{CFL}}=4.99\times10^{-14}s$. A

TABLE 1 Comparison of the CPU Time and Average Relative Error (Debye Medium)

Method	CFLN	CPU Time(s)	Average Error
Explicit	1	32.203	
Proposed method	1	76.422	0.00034062
Proposed method	2	38.844	0.00034677
Proposed method	3	25.312	0.00043720
Proposed method	4	19.156	0.00035133
Proposed method	5	15.688	0.00035474
Proposed method	7	10.891	0.00036384

modulated Gaussian pulse having significant spectral energy up to 100 GHz was used. Figure 1 depicts the reflection coefficient calculated by the proposed scheme at different CFLN along with the analytical results. Here, the $CFLN \equiv \Delta t/\Delta t_{CFL}$ with Δt being the time discretization used in the simulation. We see the proposed scheme works even when CFLN**>1** and the numerical results agree well with the analytical values. We then quantify the numerical error at higher $CFLN$ by the average relative error calculated over the whole frequency band as $\sqrt{\sum_f (\boldsymbol{R}-\boldsymbol{R}^{\mathrm{ref}})^2}/\sum_f (\boldsymbol{R}^{\mathrm{ref}})^2$ where, $\boldsymbol{R}$ is the numerically calculated reflection coefficient and $\boldsymbol{R}^{\mathrm{ref}}$ is the analytical reflection coefficient. For the numerical test of Figure 1 the average relative errors of the proposed scheme at different $CFLN$ are given in Table 1. We see that the scheme can maintain good accuracy even at higher $CFLN$. Table 1 also shows the CPU time required by the proposed scheme against the time required by the explicit FDTD method on the same computer. At $CFLN=3$ the proposed scheme becomes faster than the explicit scheme. At $CFLN=7$ the scheme becomes 3 times faster than the explicit scheme.

For the validation of the proposed scheme for Lorentz medium, we studied the transmittance of a thin silver slab. The slab is 30-nm thick and have the Lorentz parameters given in [10]: $\Delta\varepsilon_l=4.7982\times10^7-4.2167$, $\omega_l=2.0254\times10^{12}$ Hz, and $\gamma_l=1.4046\times10^{13}$ HZ. The spatial cell size was 1.5 nm. The excitation source was a Gaussian pulse with centre frequency 1500 THz. Figure 2 presents the simulated transmittance through the silver slab using the proposed scheme along with the analytical values (as reference). We see that the proposed scheme provides

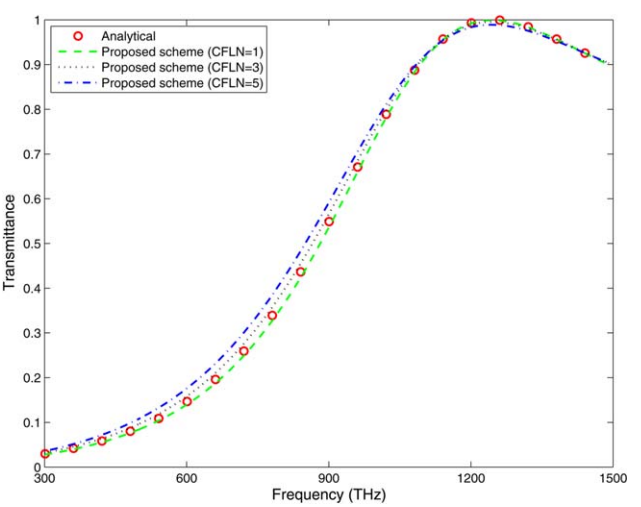

Figure 2 Transmittance of a 30-nm thick silver slab along with the analytical results (as reference). [Color figure can be viewed in the online issue, which is available at wileyonlinelibrary.com]

TABLE 2 Comparison of the CPU Time and Average Relative Error (Lorentz Medium)

Method	CFLN	CPU Time(s)	Average Error
Explicit	1	41.719	
Proposed method	1	80.500	0.0098
Proposed method	2	40.016	0.0039
Proposed method	3	27.297	0.0164
Proposed method	4	19.688	0.0283
Proposed method	5	15.781	0.0397
Proposed method	7	11.359	0.0608

an acceptable solution even for a large CFLN Average relative errors between numerical and analytical solutions at different CFLN have been displayed in Table 2. The required CPU time for computation is also shown in Table 2 indicating its notable efficiency.

4. CONCLUSION

A new unconditionally stable scattered field FDTD formulation for dispersive media characterized by Debye and Lorentz models is presented. The scheme leads to tridiagonal implicit equations but unlike ADI it does not require the mid-time field computations. Numerical tests validated unconditional stability and accuracy of the scheme. The scheme becomes faster than the explicit FDTD scheme when the CFL number is as low as 3. Average relative errors resulted from the use of larger time-step sizes beyond the Courant limit are also shown.

ACKNOWLEDGMENT

The authors wish to acknowledge the Alexander von Humboldt Foundation for the funding of this research.

REFERENCES

1. A. Taflove and S. Hagness, Computational electrodynamics: The finite–difference time–domain method, 3rd ed., Artech House, Boston, MA, 2005.
2. K. Kunz and R. Luebbers, The finite difference time domain method for electromagnetics, CRC Press, Boca Raton, FL, 1993.
3. T. Namiki, A new FDTD algorithm based on alternating-direction implicit method, IEEE Trans Microwave Theory Tech 47 (1999), 2003–2007.
4. F. Zheng, Z. Chen, and J. Zhang, A finite difference time domain method without the Courant stability conditions, IEEE Microwave Guided Wave Lett 9 (1999), 441–443.
5. S. J. Cooke, M. Botton, T. M. Antonsen, Jr., and B. Levush, A leap-frog formulation of the 3D ADI-FDTD algorithm, Int J Numer Model Electron Netw Dev Fields 22 (2009), 187–200.
6. S. C. Yang, Z. Chen, Y. Yu, and W. Yin, An unconditionally stable one-step arbitrary-order leapfrog ADI-FDTD method and its numerical properties, IEEE Trans Antennas Propag 60 (2012).
7. H. H. Abdullah, F. M. El-Hefnawi, and A. Z. Elsherbeni, A FDTD scattered field formulation for dispersive media, In: Proceedings of IEEE APS International Symposium, 16–21 July, 2000, pp. 248–251.
8. R. J. Lubbers, D. Steich, and K. Kunz, FDTD calculation of scattering from frequency dependent materials, IEEE Trans Antenna Propag 41 (1993), 1249–1257.
9. S. C. Kong, J. J. Simpson, and V. Backman, ADE-FDTD scattered field formulation for dispersive materials, IEEE Microwave Wireless Compon Lett 18 (2008), 4–6.
10. J. Olkkonen, FDTD scattered field formulation for scatterers in stratified dispersive media, Opt Exp 18 (2010).
11. H. Rouf and D. Erni, Scattered field FDTD with unconditional stability for Drude medium, IEEE Antennas Wireless Propag Lett, in press.
12. J. Roden and S. Gedney, Convolution PML (CPML): An efficient FDTD implementation of the CFS-PML for arbitrary medium, Microwave Opt Technol Lett 27 (2000), 334–339.
13. B. Donderici and F. L. Teixeira, Symmetric source implementation for the ADI-FDTD method, IEEE Trans Antennas Propag 53 (2005), 1562–1565.

A NOVEL RECONFIGURABLE ANTENNA ARRAY WITH CONTROLLABLE TUNING AND BEAM STEERING

Adrianos G. Katsouris, Christos D. Nikolopoulos, Anargyros T. Baklezos, and Christos N. Capsalis
Department of Information Transmission Systems and Material Technology, School of Electrical and Computer Engineering National Technical University of Athens, 9, Iroon Polytechniou Str, Zografou, Athens, 15773, Greece; Corresponding author: adrinkats@central.ntua.gr

Received 4 December 2015

ABSTRACT: *This article describes a reconfigurable monopole liquid antenna array, suitable for wireless communications in the UHF band, focusing on obtaining and controlling notch radiation directions. Two different implementations are being studied, at the beginning three collinear monopoles placed over a ground plane and then, five monopoles over a ground plane placed in such a manner as to form a cross. By replacing the parasitic elements with cylinders filled with conductive fluids and also surrounding the driven element, it is possible it is possible to change at will the whole antenna's layout and to control both the maximum directivity angle over the azimuth and the resonant frequency, filtering interfered channels and background noise.* © 2016 Wiley Periodicals, Inc.

Microwave Opt Technol Lett 58:1782–1786, 2016; View this article online at wileyonlinelibrary.com. DOI 10.1002/mop.29913

Key words: *reconfigurable antennas; conductive fluid; tenability; beam steering; notch radiation directions*

1. INTRODUCTION

Reconfigurable antennas have become, increasingly during the past decades, a very desirable type of antennas, in almost every field of telecommunications [1]. As technology expands over more and more people throughout the world, the demand for several means of communication, results in a corresponding increasing demand for different types of antennas. Especially at the field of portable communications, where the need for increased data transfer speeds is obvious and the use of multiple frequency bands is common, the demand for different antennas is being evident [2]. Ultra-Wideband (UWB) antennas are able to meet this demand, but they also introduce noise and interference in the link, since they cannot discriminate the wanted signals from the harmful.

Reconfigurability can also be used in order to manipulate the radiation pattern of an antenna. The coexistence of many different types of wireless networks, spectrally adjacent to each other, such as Digital Terrestrial Television, mobile communications (GSM/UMTS/LTE/WiMAX) and broadband connections (WiFi) creates the need for the base stations and the user terminals to have specific directivity characteristics, aiming at maximizing the budget of the desired wireless link and minimizing it for the others [3], in order to decrease the interference that is caused.

Recent research has shown that liquid antennas as a form of reconfigurability can achieve interesting performance and this